*Tellus (1995), 47B, 471–489*
*Printed in Belgium – all rights reserved*


**TELLUS**
*ISSN 0280–6509*

# Impact of drought stress and other factors on seasonal land biosphere $CO_2$ exchange studied through an atmospheric tracer transport model

By WOLFGANG KNORR* and MARTIN HEIMANN, *Max-Planck-Institut für Meteorologie, Bundesstr. 55, 20146 Hamburg, Germany*

(Manuscript received 10 February 1994; in final form 20 February 1995)

ABSTRACT

We develop a simple, generic global model of carbon cycling by terrestrial vegetation driven by climate data, observed greenness from global vegetation index data, and a drought-stress indicator calculated with a one-layer bucket model. Modelled $CO_2$ fluxes are then fed into a three-dimensional atmospheric tracer transport model, so that results can be checked against observed concentrations of $CO_2$ at various monitoring sites. By exploring a wide range of model formulations, we find an optimal fit of the model to atmospheric $CO_2$ data. To check these results, we use a second model with a coupled photosynthesis-hydrology scheme, using the Penman-Monteith equation to calculate evapotranspiration. This model simulates feedbacks between drought-stress and photosynthesis through the soil-water balance. We show that $CO_2$ measurements at tropical and southern-hemisphere stations can be used to constrain the seasonal atmosphere-biosphere carbon exchange in the wet-dry tropics. In both models, this seasonality is strongly suppressed, more strongly in fact than predicted by some complex terrestrial-vegetation models. We also find some evidence of a considerable $CO_2$ release from soils during the northern-hemisphere winter. An exponential air-temperature dependence of soil release with a $Q_{10}$ of 1.5 is found to be most appropriate, with no cutoff at low freezing temperatures. The results of this study should indicate in how far measurements of atmospheric $CO_2$ concentration can provide a constraint on global models of terrestrial-vegetation activity.

## 1. Introduction

The terrestrial biosphere is one of the dominant factors controlling the global carbon cycle. Therefore, models are required that can reliably simulate carbon uptake and release by terrestrial plants and soils on a global scale. One approach to developing such models is to represent known physiological mechanisms within a computer program, and calibrating various parameters with the help of measurements from test sites (Raich et al., 1991; Potter et al., 1993). However, differences between such models reflect not only discrepancies in input data, but also uncertainties involved in the process of extrapolating site-specific results to the global scale.

In this study, we choose a different route: we develop a simple, generic global model using measurements of atmospheric $CO_2$ concentration as a constraint. The model is diagnostic by using observed greenness from satellite measurements as input. A one-layer bucket model using vegetation-independent estimates of evapotranspiration is used to account for water stress in plants. Predicted $CO_2$ fluxes are fed into an atmospheric tracer transport model and compared with the seasonal cycle of $CO_2$ concentration measured at various monitoring sites. We explore a wide range of model formulations, to assess how sensitive this test is against changes in model parameters and

* Corresponding author.

formulations, eventually to find a best-fit solution.

In addition, we use a second vegetation model, with a coupled hydrology-photosynthesis scheme, using the more physically based Penman-Monteith equation for evapotranspiration (Knorr et al., 1995). Here, carbon uptake and release are directly linked through stomatal closure, which is controlled by incident radiation, vapour-pressure deficit, and soil water. This model will be referred to as Model 2, whereas the former will be called Model 1 throughout the text.

We choose a simple, generic model, because such a model is much easier to modify than more sophisticated global models. The results should also reflect the information provided by the atmospheric data, and therefore be as independent as possible of specific site measurements. In this way, they may be able to serve as an independent test for global mechanistic ecosystem models (Janacek et al., 1991; Potter et al., 1993; Raich et al., 1991; Running and Hunt, 1993).

## 2. Data and procedures

As climatic input data we use two data sets: First, the climatology by Cramer and Leemans (pers. comm.), an improved version of the IIASA data base by Leemans and Cramer (1991), with monthly values of temperature, precipitation and cloudiness. Second, monthly means of temperature, precipitation, solar and thermal radiation from short-range weather forecasts by the European Centre for Medium Range Weather Forecasts (ECMWF; Arpe, 1991) for the years 1986 and 1987 (matching the wind data, see below). Solar incident radiation, $I$, is estimated from cloudiness following Linacre (1968), whereas net radiation is calculated according to Stanhill et al. (1972; see Section 8 for more details), except when using the ECMWF data, where solar and thermal radiation are provided directly. In addition, Model 2 requires global fields of relative humidity (Leemans and Cramer, 1991). As observed greenness we use the Normalized Difference Vegetation Index (NDVI) measured on board the NOAA-9 satellite (Gallo, 1992). It has been demonstrated that the NDVI, defined as the difference of the reflectivities in the near-infrared minus red divided by their sum, is a reasonable indicator of photosynthetic efficiency of vegetation formations under non-stress conditions (Kumar and Monteith, 1981; Tucker and Sellers, 1986; Myneni et al., 1992; Asrar et al., 1992). We take 3 years of monthly maxima (May 1985 to April 1988) to reduce the influence of cloud contamination. The data are corrected for sensor degradation according to a method by Los (1993). For lack of calibration data, we do not use data from the ensuing NOAA-11 platform. The mean annual course of NDVI is taken in combination with the Cramer and Leemans (CL) climatology, whereas data from 1986 and 1987, respectively, are used with the ECMWF climate input.

Observed atmospheric $CO_2$ concentrations are taken from the NOAA Climate Monitoring and Diagnostic Laboratory's flask sampling program (Conway and Tans, 1990; CDIAC, 1991). The mean seasonal cycle and the variance of the monthly values are computed from data records of 1980 to 1990, as far as they are available, by subtracting the long-term trend, which itself is fitted to the annual means of the data records using Hermite cubics.

Both vegetation models, and the bucket model used with Model 1, have a spatial resolution of 0.5°, whereas the atmospheric tracer transport model, TM2, a modified version of the one developed by Heimann and Keeling (1989), has a resolution of 7.83° by 10.00°, with 9 layers in the vertical (Heimann, 1995). We calculate a mean annual course of atmosphere-biosphere $CO_2$ exchange at monthly time steps, assuming that at each pixel the net exchange is zero over one year, thus excluding the effect of any interannual changes in the carbon balance of vegetation and soils. Internally, Model 1 has a basic time step of one month, the bucket model executed in conjunction with Model 1 (see Section 8) of one day, and Model 2 of one hour.

Next, the monthly fluxes from both models are aggregated in space to the TM2 grid, and interpolated to daily fluxes, again using Hermite cubics. TM2 is run with wind data from ECMWF analyses, both from 1986 and 1987, and uses the mass-flux scheme by Tiedtke (1989) for vertical mixing by cumulus clouds. Eventually, monthly means of $CO_2$ concentration are extracted at those TM2 grid boxes representing various monitoring sites, and compared to the detrended annual variation in the measurements.

## 3. Model development and simulations

### 3.1. Test criteria

In order to assess the goodness-of-fit of each model formulation, we develop two different test criteria. Since in northern mid and higher latitudes, the seasonal cycle is strongly dominated by fluxes from the terrestrial biosphere (cf. Heimann et al., 1989; Nakazawa et al., 1993), we define a cost function, $J$, measuring the weighted difference between simulated (terrestrial biospheric) $CO_2$ concentrations and measurements:

$$J=\frac{1}{n}\sum_{i=1}^{n}\frac{(c_{i,\,\mathrm{obs}}-c_{i,\,\mathrm{sim}})^2}{s^2_{i,\,\mathrm{obs}}}; \qquad (1)$$

$i$ runs over 12 months times 5 stations as listed in Table 1, and $c_{i,\,\mathrm{obs}}$ and $c_{i,\,\mathrm{sim}}$ are observed and simulated $CO_2$ concentration of the mean seasonal cycle with the convention that the sum over one year equals zero. All stations belong to the NOAA CMDL flask sampling programme (see above), have a long record of measurements, and lie sufficiently far north to neglect the influence of oceanic fluxes and emissions from fossil fuel burning and land-use change on the seasonal cycle of $CO_2$.

Such additional factors, however, introduce a seasonal cycle of similar size as that caused by terrestrial-biosphere fluxes at tropical and southern latitudes (Heimann et al., 1989). Here, we use records of the years 1980 to 1990 from Ascension Island (ASC, 8°S, 14°W), and of 1985 to 1990 from Cape Grim, Tasmania, (CGO, 41°S, 145°E). We take CGO to represent the southern mid latitudes, whereas ASC is ideally situated to receive the $CO_2$ signal from the tropical and subtropical vegetation of southern Africa. To account for the influence of oceanic sources, we present results calculated with a plankton model included into an ocean general-circulation model by Kurz (1993), coupled to the TM2. Their model correctly predicts the seasonal cycle of the $O_2/N_2$ ratio at CGO, which gives a good indication of the accuracy of the predicted $CO_2$ seasonality. Industrial $CO_2$ sources of 5.661 GtC annually, the value for 1987 (CDIAC, 1991), with a prescribed temporal distribution as in Heimann and Keeling (1989), are also fed into the TM2 to account for this additional factor. We do not simulate the effect of land-use change (cf. Heimann et al., 1989) and of biomass burning. However, published simulation results by Iacobellis et al. (1994, Fig. 5b), who have used a similar transport model, show an amplitude of about 1 ppmv at 3.9°S, 50°W from biomass burning in the tropics, with a peak in August and a trough in April. We expect a similar signal to arrive also at ASC.

As a second test criterion, we only consider the amplitude of the simulated seasonal cycle at ASC and CGO. If a specific formulation of the biosphere model produces an amplitude that is considerably larger than observed so that the additional sources could not account for that difference, it is rejected.

### 3.2. Model 1

This is the main biosphere model used to explore a wide range of formulations tested according to the criteria of the previous subsection. We formulate only two carbon fluxes, one for $CO_2$ uptake by plants, i.e., net primary productivity (NPP), and one return flux from the soil and plant litter to the atmosphere, subsumed under soil respiration (SR). The approach is similar to the studies by Fung et al. (1987) and Heimann and Keeling (1989), with the exception of using an additional drought-stress factor. Following Monteith (1977), we assume that NPP is linearly related to the amount of photosynthetically active

Table 1. *Monitoring stations used for computing the cost function, J, from north to south*

| Station | Code | Latitude | Longitude | Height [m] | Period |
|---|---|---|---|---|---|
| Point Barrow | BRW | 71.3°N | 156.6°W | 11 | 1980–1990 |
| Ocean Station "M" | STM | 66.0°N | 2.0°E | 6 | 1982–1990 |
| Cold Bay | CBA | 55.2°N | 162.7°W | 11 | 1980–1990 |
| Terceira Island, Azores | AZR | 38.8°N | 27.1°E | 30 | 1980–1990 |
| Cape Kumukahi, Hawaii | KUM | 19.5°N | 154.8°W | 3 | 1980–1990 |

radiation (PAR) absorbed by the plant canopy. We estimate the fraction of absorbed PAR (FPAR, i.e., absobed PAR divided by incident PAR) from a linear regression for a medium-bright soil background derived theoretically by Asrar et al. (1992) for both closed and clumped vegetation formations. However, atmospheric effects reduce the value of the NDVI as measured by the satellite by around 40% to maximum values of typically 0.5. We assume that a NDVI of 0.5 corresponds to a maximum value of FPAR of 0.9. The resulting regression equation is

$$\mathrm{FPAR} = 1.222(\mathrm{NDVI}/0.559 - 0.1566). \quad (2)$$

Values of FPAR above 0.9 are assumed 0.9, negative values are asssumed zero. Similar regression equations derived from both model simulations and field measurements can be found in Ruimy et al. (1994). Other authors have derived a similar linear relationship between the simple-ratio vegetation index (SRVI, defined as reflectance in the infrared divided by red) and unstressed canopy photosynthesis (Tucker and Sellers, 1986; Sellers et al., 1992), and a field study by Verma et al. (1993) supports this assumption. However, the number of studies that report a linear correlation between FPAR and NDVI is considerably larger than for the SRVI, as reported by Ruimy et al. (1994).

In addition, we use a modified version of a one-layer bucket model developed by Prentice et al. (1993) to obtain a measure of drought stress (see Section 8). By using equilibrium evapotranspiration, which is independent of vegetation, as estimate of evaporative demand the bucket model can be run independently of Model 1. The Priestley-Taylor ratio, $\alpha$, defined as actual divided by potential evapotranspiration, is then used as a drought-stress indicator. Accounting for the uncertainty in how far plants can reduce $CO_2$ uptake under conditions of drought stress while maintaining high FPAR (seen as high NDVI), we test two formulations for NPP, only one containing the drought-stress factor:

$$\mathrm{NPP} = A \times \alpha \times \mathrm{FPAR} \times \mathrm{PAR}, \quad (3a)$$

$$\mathrm{NPP} = A \times \mathrm{FPAR} \times \mathrm{PAR}. \quad (3b)$$

PAR is assumed to be half of $I$, the solar incident radiation ($\mathrm{W\,m^{-2}}$). $A$, the light-use efficiency (gC/MJ PAR), is assumed globally constant (1 gC = 1 g carbon). We leave the size of $A$ (gC/MJ PAR) open and use it as a global fitting parameter.

In formulating soil respiration, we follow Bonan (1991) and Norman et al. (1992) who both used soil moisture times an exponential function of soil temperature, apart from minor additional factors. Bonan, referring to various field studies (Vogt et al., 1980; Moore, 1983; Stohlgren, 1988; Taylor and Jones, 1990), assumes that the exponential dependence is still valid for low freezing temperatures. In this study, we replace soil temperature with surface air temperature, and soil moisture with the Priestley-Taylor ratio, $\alpha$, which follows soil moisture closely in the one-layer bucket model. However, since it it is not clear how water availability relates quantitatively to microbial activity in the soil, we also consider a formulation without a drought-stress factor. Additionally, we test the effect of introducing a low-temperature cutoff at $-10°\mathrm{C}$, as used in Heimann and Keeling (1989), and at varying temperature through a linear dependence by Fung et al. (1987). We combine these different assumptions, and obtain four alternative formulations:

$$\mathrm{SR} = B \times \alpha \times Q_{10}^{T/10} \quad (4a)$$

$$\mathrm{SR} = \begin{cases} B \times \alpha \times Q_{10}^{T/10} & \text{for } T \geqslant -10°\mathrm{C} \\ 0 & \text{for } T < -10°\mathrm{C} \end{cases} \quad (4b)$$

$$\mathrm{SR} = B \times Q_{10}^{T/10} \quad (4c)$$

$$\mathrm{SR} = \begin{cases} B \times Q_{10}^{T/10} & \text{for } T \geqslant -10°\mathrm{C} \\ 0 & \text{for } T < -10°\mathrm{C} \end{cases} \quad (4d)$$

$T$ is the surface air temperature, $Q_{10}$ an empirical constant, and $B$ is determined by the condition that SR and NPP balance over one year in each grid cell. (Unlike $A$, $B$ is not globally constant.) Measured values of $Q_{10}$ have been found between 1.3 and 3.3 (Raich and Schlesinger, 1992), they are, however, related to soil temperature, while Heimann and Keeling use air temperature and $Q_{10} = 1.5$. In this study, we leave the size of $Q_{10}$ open and take it as a second global fitting parameter.

### 3.3. *Model 2*

In this second vegetation model, $CO_2$ and water fluxes are simultaneously controlled by extractable soil moisture through stomatal closure. This is, therefore, a coupled carbon and water flux model,

with a one-layer soil compartment as in the bucket model used with Model 1. It starts by calculating the photosynthetic rate under unstressed conditions, $A_u$ (mol[$CO_2$] $m^{-2} s^{-1}$), from incident PAR (in mol[photons] $m^{-2} s^{-1}$) at an hourly time step, assuming a globally constant quantum efficiency, $\varepsilon$, defined as the ratio of $CO_2$ molecules photosynthesized by the leaf per photons absorbed:

$$A_u = \varepsilon \times \mathrm{FPAR} \times \mathrm{PAR}. \quad (5)$$

FPAR is calculated from NDVI as in Model 1, and PAR is again assumed half of $I$. The canopy conductance, $g_c$, is then calculated that just allows this photosynthetic rate through the stomatal openings by assuming a fixed value for the $CO_2$ concentration difference between the leaf interior and ambient air (70% of the mean atmospheric concentration, i.e., 249 ppmv, similar to Running 1984). $g_c$ is then multiplied by factors accounting for vapour-pressure deficit, $\Delta e$ (Pa):

$$f(\Delta e) = \frac{1}{1 + b_e \Delta e}, \quad (6)$$

and extractable soil moisture, $w$ (mm):

$$f(w) = \frac{1 - \exp(-b_w(w/w_{\max}))}{1 - \exp(b_w)} \quad (7)$$

(Kim and Verma, 1991). We take $b_e = 3.0 \times 10^{-4}\ \mathrm{Pa}^{-1}$ and $b_w = 3.0$ after checking against data by Turner et al. (1984) and Gollan et al. (1985). $w_{\max}$ (mm) is computed as in the bucket model (see Section 8). Finally, canopy conductance determines both photosynthesis, and water loss through the Penman-Monteith equation (Monteith, 1965), assuming perfect stomatal control, i.e., water loss takes place only during carbon uptake, and neglecting soil evaporation. Aerodynamic resistance is fixed at $20\ \mathrm{s\ m}^{-1}$, higher than the value used by Running and Coughlan (1988) in their forest model ($5\ \mathrm{s\ m}^{-1}$), but probably more appropriate for grasslands and savannas, where most of the water limitation is expected to occur.

The photosynthetic rate is integrated to monthly values of net daytime leaf uptake (NDLU), which is gross primary productivity (GPP) minus daytime leaf respiration. To obtain NPP, we assume that remaining plant respiration is 40% of NDLU resulting when soil moisture is not limiting. In order to estimate GPP, we further assume that daytime leaf respiration is 1/3 of total plant respiration, or 20% of NDLU under no drought stress. Again under non-stress conditions, this amounts to GPP = 1.2 NDLU, and NPP = 0.5 GPP. This agrees with findings by Ryan (1991) that total plant respiration is typically 50% of GPP. Soil respiration is modelled as in Model 1, eq. (4a), except that $\alpha$ is replaced by extractable soil water. Incident radiation, $I$, and the canopy radiative balance, $R_n$, are calculated as in the bucket model (see Section 8). $\varepsilon$ and $Q_{10}$ are used as fitting parameters. More details of Model 2 can be found in Knorr et al. (1995).

### 3.4. *Simulations*

We run a variety of simulations with Model 1 using different combinations of eqs. (3a) and (3b) for NPP and (4a) to (4d) for SR, with values for $Q_{10}$ varying between 1.0 and 2.4 (see Table 2). Wind data are taken both from 1986 and 1987. With $B$ determined locally by the condition of flux balance over one year, the remaining undetermined global parameter is $A$. Since tracer transport can be assumed linear, $A$ only serves as a scaling factor for the simulated concentrations $c_{i,\mathrm{sim}}$ in eq. (1). Therefore, we fit $A$ after each run analytically by minimizing $J$.

To assess the sensitivity to the particular climatology and NDVI data set used, we also run Model 1 with the ECMWF forecasts of 1986 and 1987, combined with NDVI and winds of the same year, using Formulation I (i.e., combining eqs. (3a) and (4a)).

Because of feedbacks between photosynthesis and the soil water balance, fitting $\varepsilon$ in Model 2 cannot be done analytically, but must be achieved by an iterative procedure. Thereby we assume that to a first approximation, a small change in $\varepsilon$ does not change the water balance. In this case the net atmosphere-biosphere $CO_2$ exchange depends linearly on $\varepsilon$, so that $\varepsilon$ can be fitted in the same way as $A$ in Model 1. Starting with a value of 0.020, this linear fit is then used as a new estimate in the next iteration step. The method converges well to a minimum in $J$ and requires typically two to three simulation cycles of consecutively running Model 2 and the transport model, TM2.

Table 2. *Results of the simulations to test the various formulations of NPP and SR and a range of values for $Q_{10}$*

| Formulation | NPP eq. | SR eq. | $Q_{10}$ | Winds | $J$ | $A$ | glNPP |
|---|---|---|---|---|---|---|---|
| I | 3a | 4a | 1.2 | 1987 | 3.56 | 0.50 | 44 |
| | α | α | 1.5 | | 2.69 | 0.68 | 60 |
| | | | 1.9 | | 3.84 | 0.96 | 85 |
| | | | 2.4 | | 10.62 | 1.31 | 115 |
| | | | 1.2 | 1986 | 3.90 | 0.50 | 44 |
| | | | 1.5 | | 3.09 | 0.67 | 59 |
| | | | 1.9 | | 4.07 | 0.95 | 84 |
| | | | 2.4 | | 10.27 | 1.30 | 114 |
| II | 3a | 4b | 1.0 | 1987 | 2.88 | 0.60 | 52 |
| | α | α | 1.2 | | 3.01 | 0.71 | 62 |
| | | cutoff | 1.5 | | 4.04 | 0.90 | 79 |
| | | | 1.9 | | 7.75 | 1.16 | 102 |
| III | 3a | 4c | 1.2 | 1987 | 3.79 | 0.52 | 45 |
| | α | | 1.5 | | 2.75 | 0.71 | 62 |
| | | | 1.9 | | 3.33 | 1.03 | 91 |
| IV | 3a | 4d | 1.0 | 1987 | 3.99 | 0.60 | 53 |
| | α | cutoff | 1.2 | | 3.90 | 0.73 | 64 |
| | | | 1.5 | | 4.49 | 0.95 | 83 |
| V | 3b | 4a | 1.2 | 1987 | 3.97 | 0.40 | 46 |
| | | α | 1.5 | | 3.24 | 0.54 | 62 |
| | | | 1.9 | | 4.84 | 0.75 | 86 |
| VI | 3b | 4b | 1.0 | 1987 | 2.97 | 0.47 | 54 |
| | | α | 1.2 | | 3.14 | 0.56 | 64 |
| | | cutoff | 1.5 | | 4.38 | 0.70 | 81 |
| VII | 3b | 4c | 1.2 | 1987 | 3.74 | 0.44 | 50 |
| | | | 1.5 | | 2.60 | 0.61 | 70 |
| | | | 1.9 | | 3.60 | 0.89 | 102 |
| | | | 2.4 | | 11.89 | 1.22 | 140 |
| | | | 1.2 | 1986 | 4.05 | 0.43 | 50 |
| | | | 1.5 | | 3.07 | 0.60 | 69 |
| | | | 1.9 | | 4.05 | 0.87 | 100 |
| | | | 2.4 | | 11.71 | 1.20 | 138 |
| VIII | 3b | 4d | 1.0 | 1987 | 3.49 | 0.50 | 57 |
| | | cutoff | 1.2 | | 3.24 | 0.61 | 70 |
| | | | 1.5 | | 3.79 | 0.80 | 92 |
| | | | 1.9 | | 7.50 | 1.07 | 123 |

In each line we give the value of the cost function, $J$, after optimizing the global photosynthetic efficiency, $A$, (gC per MJ PAR). The value for global annual NPP (glNPP), in GtC, is also displayed. The error in $A$ resulting for uncertainties in the observed $CO_2$ concentration is generally around 1.1%.

## 4. Results

### *4.1. First test criterion*

The results of various seasonal-cycle simulations after optimizing $J$ with Model 1 using CL climatology are listed in Table 2. Measured and simulated seasonal cycles of $CO_2$ are shown in Fig. 1 for the stations used to calculate $J$. We have added Kotelny Island in North Siberia (76°N, 138°E), with measurements from 1987 to 1990 by Brounshtein et al. (1988). Table 2 includes the NPP and SR formulation chosen, $Q_{10}$, the optimized value for $J$, the corresponding value of $A$ (gC/MJ PAR), and the resulting global annual NPP

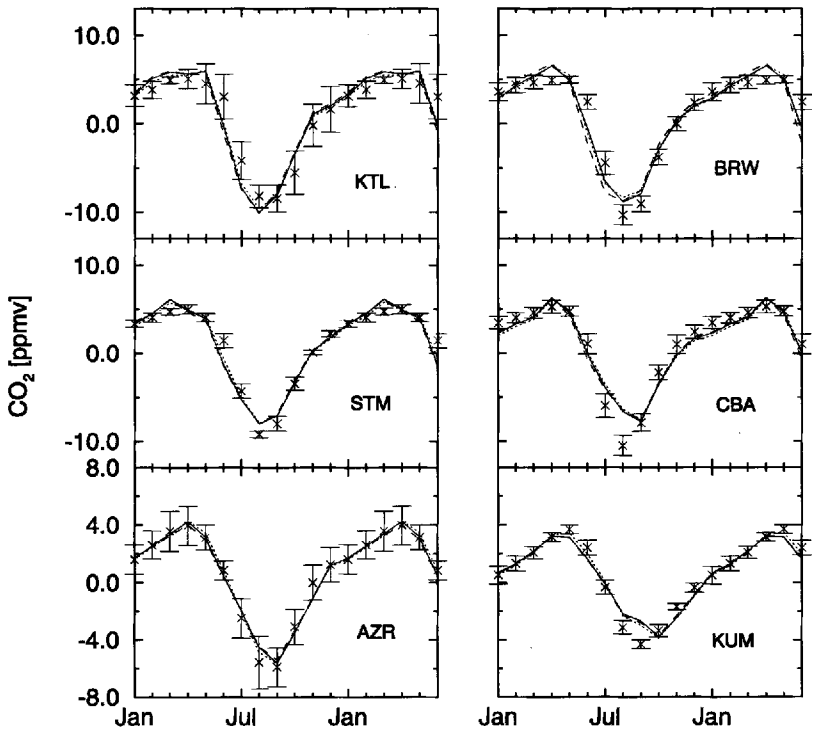


*Fig. 1.* Simulated and observed seasonal cycle at those stations used for calculating the cost function, $J$, plus Kotelny Island (KTL, 76°N, 138°E), for Formulations I (full curves) and VII (dotted) and for Model 2 (dashed), with $Q_{10} = 1.5$, using 1987 winds. Observations, $c_{i,\,obs}$, are shown with error bars indicating $s_{i,\,obs}$. The first half of the annual cycle is repeated for display purposes.

(glNPP) in GtC (1 GtC = $10^{12}$ kg carbon). The error in $A$ at fixed $Q_{10}$ that results from the uncertainty, $s_{i,\,obs}$, in the observed values, $c_{i,\,obs}$, is about 1.1 % for all cases.

All simulated seasonal cycles in Fig. 1 agree well with observations. However, the model often fails to match the lowest $CO_2$ concentration during summer. Further, the model leads observations by about half a month at the most northern stations, where the seasonal cycle is most pronounced (cf. Subsection 4.3). The differences between the simulations displayed are generally small (Model 1, Formulations I and VII, and Model 2). They result mainly from the way drought stress is included in the $CO_2$ flux formulation. This indicates that water availability has only a small impact on the seasonal cycle at northern mid and higher latitude stations.

There are 3 variations tested in these simulations: of the soil-respiration parameterization, of inclusion of the drought-stress factor, $\alpha$, and of the wind data used. Considering the first variation, we find a clear optimum around $Q_{10} = 1.5$ when no low-temperature cutoff is applied, independent of wind data, NPP and SR formulation. However, with a cutoff at −10°C, the optimum shifts to values around 1.0 to 1.2. Such values appear to be unreasonably low, since they imply that in northern latitudes, the seasonality of SR is almost entirely determined by freezing and thawing. It seems that a considerable amount of carbon released during northern-hemisphere winters is required in order to match the atmospheric $CO_2$ records, either through a small temperature dependence of SR, or through decomposition even under conditions of severe frost.

Regarding the other two variations, the uncertainties resulting from changes in the wind field appear to be of similar size as the effect of changing the way the drought-stress factor is included in

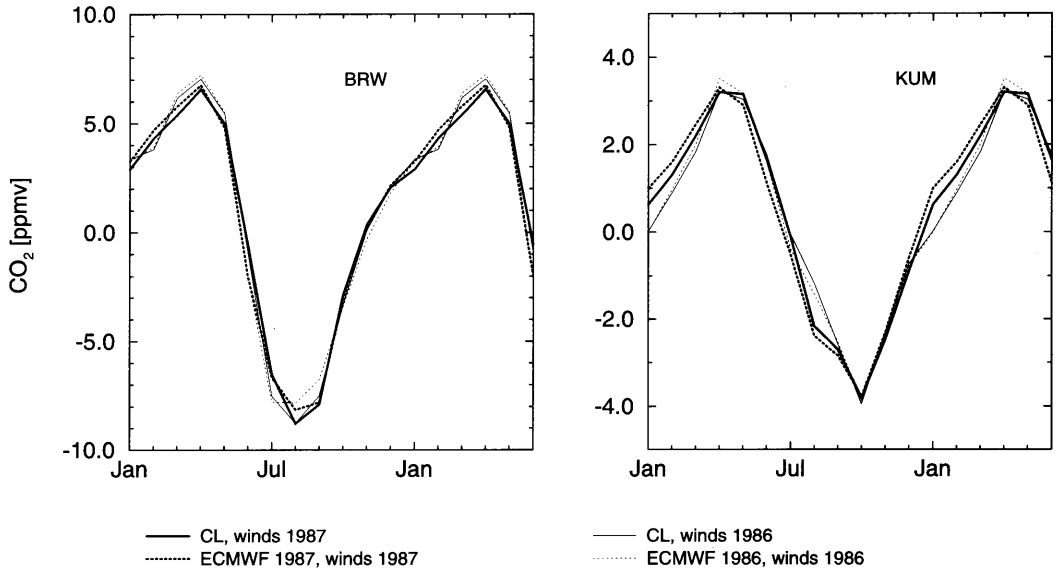


*Fig. 2.* Simulated seasonal cycle of $CO_2$ using Formulation I and $Q_{10} = 1.5$ for various climate and wind data. CL denotes climatology by Cramer and Leemans. Simulations with ECMWF short-range forecasts were done with only one year of climate and NDVI data (1986 or 1987).

the carbon-flux formulations. Consequently, we arrive at a negative conclusion: atmospheric $CO_2$ measurements in the northern high and mid latitudes deliver no constraint on modelling drought-stress in terrestrial vegetation. Fig. 2 also suggests that changing the wind data has a larger impact on simulations than changing the climate and NDVI data, since the curves derived from the same wind data lie generally closer together than the curves derived from the same climate and NDVI data, although the differences between the curves are generally small.

We note, however, that including $\alpha$ into NPP results in an increase in estimated global annual NPP from around 60 GtC to about 70 GtC when comparing Formulations I and VII, which both achieve almost the same goodness-of-fit. On the other hand, the value for $A$ found for Formulation VII is smaller than for Formulation I. This illustrates that only net fluxes are tested through atmospheric transport, and that an increase in NPP accompanied by a simultaneous increase in SR is invisible for atmospheric $CO_2$ records. In general, our estimates of global annual NPP are within the range of previously found values, or slightly higher, e.g., 45 GtC by Fung et al. (1983), 47 GtC by Lieth (1975), 48 GtC by Potter et al. (1993), 60 GtC by Olson et al. (1983), and approximately 60 GtC by Ruimy et al. (1994).

We find a light-use efficiency, $A$, well within the lower range of usual measurements for crops, typically 1 to 3 g dry matter per MJ absorbed PAR, or 0.5 to 1.5 gC/MJ PAR (Prince, 1991; Ruimy et al., 1994). However, natural vegetation usually achieves only about half of typical values for crops. Ruimy et al. assign a mean value 1.01 g dry matter/MJ PAR to deciduous forests, 1.26 to grasslands, and 2.07 to crops. Assuming 45% carbon content of dry matter, this translates into 0.45, 0.57, and 0.93 gC/MJ PAR, respectively. An even lower value for maximum light-use efficiency has been fitted to various site measurements by Potter et al. (1993), who used 0.39 gC/MJ PAR in their global vegetation model, CASA. Wofsy et al. (1993) measured a light-use efficiency of 1.10 gC/MJ PAR related to GPP for a deciduous forest in Massachusettes, which, assuming 40% for total respiration costs, amounts to 0.66 gC/MJ PAR in NPP terms, close to our estimates.

Results from the simulations using ECMWF climate input with Model 1, and CL climatology with Model 2 are shown in Table 3. Despite the

Table 3. *The first simulation displayed in this table is done with Formulation I of Model 1, using ECMWF short-range forecasts from the same year as the wind data; further, results with Model 2 are shown, indicating the cost function, J, after iterative optimization of the quantum efficiency, ε (next column)*

| Simulation | | ECMWF 1987/1986 | | | Model 2 | | | | |
|---|---|---|---|---|---|---|---|---|---|
| $Q_{10}$ | winds | $J$ | $A$ | (glNPP) | $J$ | $\varepsilon$ | (glNPP) | (glGPP) | (glNPP/glGPP) |
| 1.2 | 1987 | 3.86 | 0.55 | 43 | 3.79 | 0.0157 | 46 | 93 | 0.496 |
| 1.5 | | 2.91 | 0.75 | 59 | 3.10 | 0.0219 | 64 | 129 | 0.492 |
| 1.9 | | 4.89 | 1.05 | 83 | 5.70 | 0.0312 | 88 | 182 | 0.483 |
| 1.2 | 1986 | 4.88 | 0.52 | 43 | 4.12 | 0.0155 | 46 | 92 | 0.496 |
| 1.5 | | 3.96 | 0.71 | 59 | 3.54 | 0.0214 | 62 | 126 | 0.492 |
| 1.9 | | 4.69 | 1.04 | 87 | 6.00 | 0.0306 | 86 | 178 | 0.484 |

glNPP and glGPP denote global annual NPP and GPP. The uncertainty in $A$ and $\varepsilon$ as a result of variations in measured $CO_2$ is again $\approx 1.1\,\%$.

fact that only one year of input data enters the ECMWF simulation, we find much the same results as with the CL data (see also Fig. 2). Note, however, that the values for $A$ are generally higher, a consequence of low solar radiation computed by the forecast model's radiation scheme. The latter was replaced in May 1989, resulting in overall higher values (Mocrette, 1990). Frequent adjustment of various model components are one of the problems with using data from routine forecast models. However, Arpe (1991) shows that the ECMWF model achieves precipitation forecasts in good agreement with climatological data. Further, our test is merely intended to demonstrate the robustness of the conclusions arrived at using CL climatology. Because of changes in the forecast model, caution is required when interpreting differences between the 1986 and 1987 simulations as interannual variability.

Results with Model 2 are also close to the main simulations listed in Table 2 (see also Fig. 1). Again, we find little impact of drought stress globally, considering that global NPP is just under 50% of global GPP in all cases, which is the value assumed if soil moisture is not limiting. If we had chosen a smaller value for the aerodynamic resistance, one which is more appropriate for forests (see Subsection 3.3), simulated drought stress would have been even smaller. The optimized value for the efficiency $\varepsilon$ of 0.022 expressed (gC per MJ PAR) is 1.21, assuming 4.6 mol photons per MJ PAR (Sellers et al., 1992) and 12 gC per mol $CO_2$. If we take 40% for additional respiration costs (see Subsection 3.3), we arrive at a NPP light-use efficiency of 0.73 gC/MJ, higher than found in Model 1. This value, however, is substantially reduced by a factor accounting for vapour-pressure deficit (eq. (6)).

Summarizing, the results from applying the first test criterion are twofold: we are not able to distinguish between different drought-stress schemes, however, it is possible to fit two parameter values, $A$ (or $\varepsilon$) and $Q_{10}$, irrespective of other variations investigated.

### *4.2. Second test criterion*

Fig. 3 shows simulation results for the stations ASC and CGO, with additional fluxes from the oceans and from fossil fuel burning. Terrestrial biospheric fluxes are from Model 1, Formulations I, III, V and VII (all using no cutoff, which has virtually no effect on the seasonal cycle at those stations), and from Model 2, all with $Q_{10} = 1.5$. It should be noted, however, that the influence of biomass burning is not included. As mentioned before (Subsection 3.1), we expect an amplitude of around 1 ppmv at ASC, with a trough in April and a peak in August, if savanna fires are the dominant contributor (Iacobellis et al., 1994).

Comparing the amplitudes of the observed and simulated signals, we find that both Formulation III and V clearly fail the second test criterion. It is interesting that III does not fail at CGO, whereas V fails at both stations. At ASC, the results demonstrate the opposite seasonality of $CO_2$ fluxes simulated for tropical drought-seasonal vegetation in the two formulations, since seasonal variations are mainly introduced by $\alpha$,

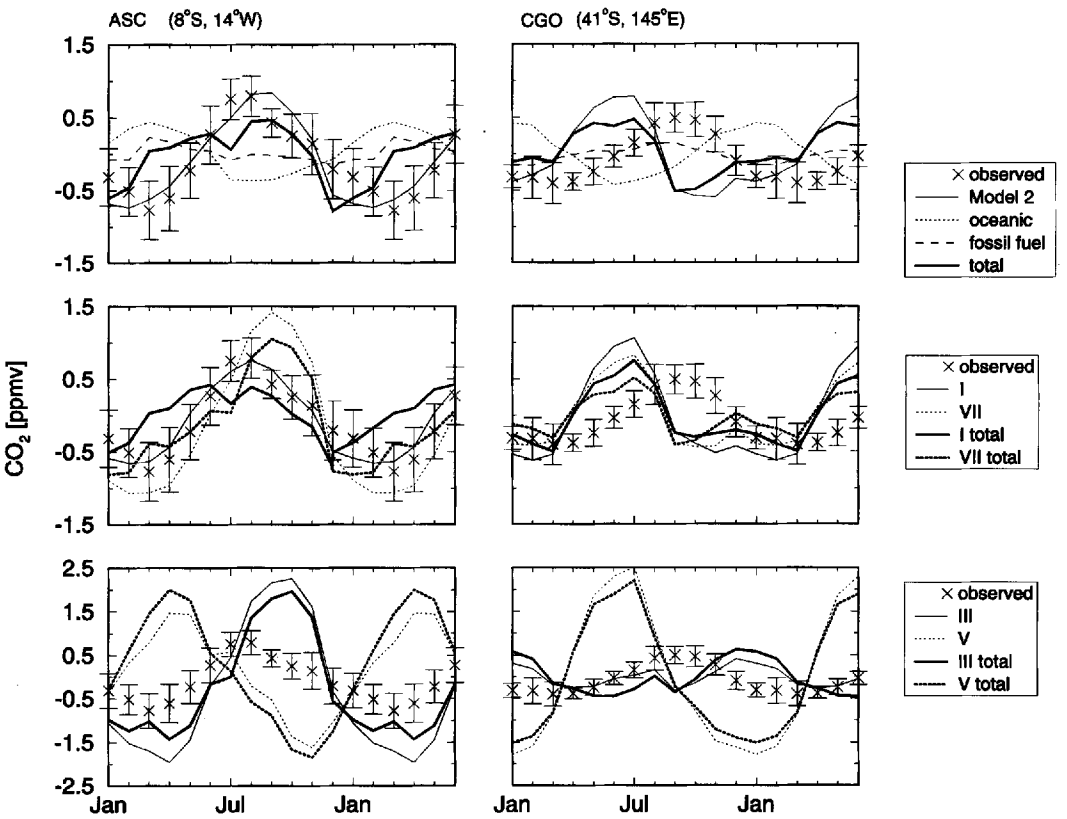


*Fig. 3.* Simulated and observed seasonal cycle at 2 southern-hemisphere stations, Cape Grim (CGO, 41°S, 145°E) and Ascension Island (ASC, 8°S, 14°W) for all formulations not using a low-temperature cutoff. Error bars for observed values indicate $s_{i,\,obs}$. We further show the simulated seasonal cycles resulting from fossil fuel burning (of a total of 5.6 GtC), and of oceanic $CO_2$ sources and sinks, including the marine biosphere. We do not include the effect of biomass burning, which is expected to introduce an additional signal of approx. 1 ppmv amplitude at ASC, with a peak in August and a trough in April.

which modulates only $CO_2$ uptake in III, and only release in V. The same is true for CGO as far as the signal coming from tropical summer-rain vegetation is concerned. An additional signal from southern temperate vegetation either adds to the tropical signal (V), or both nearly cancel each other (III).

Further, we find that Model 2 and Formulation I agree closely. Both pass the second test criterion, as is Formulation VII. In fact, all three simulations give similar results at CGO, owing to the influence of temperate vegetation, where drought-stress has little impact.

As explained above, if biomass burning was included, the total simulated signal at ASC is expected to increase by approximately 0.5 ppmv around August, and decrease by a similar amount around April. This would deteriorate the agreement of Formulation VII with observations, whereas Formulations I and Model 2 would agree better. In particular, the peak in August–September of the signal from VII appears to be too pronounced. As we will discuss in more detail in Subsection 5.1, a possible explanation is that $CO_2$ release during the dry season is still too high in Formulation VII. In contrast, at CGO none of the models agree as closely with observations. We have, however, not considered the effect of selecting specific wind directions for the days on which $CO_2$ flask samples were taken at CGO. In fact,

simulations by Ramonet (1994) show that if this effect is considered, the peak of the seasonal cycle shifts from August to September, and agreement with observations is considerably improved.

Overall, we find that atmospheric $CO_2$ concentrations measured at tropical and southern-hemisphere stations can in fact be used as a constraint on global modelling of drought-stress in plants, although not in a quantitative way, owing to the uncertainties introduced by other $CO_2$ sources.

### *4.3. General model performance*

It can been seen in Figs. 1 and 2, that at a number of stations the maximum depletion of $CO_2$ during summer is poorly matched in the model. We suggest that this can at least partly be explained by the presence of local vegetation that cannot be adequately represented at the coarse resolution of the TM2. Also, simulations generally lead observations by up to one month during the spring depletion of $CO_2$, which is probably the result of the monthly NDVI maximization that has a bias towards choosing values from later in the month when greenness is increasing. An additional reason could be high maintenance respiration and low carbon uptake during build-up of vegetation in spring.

In addition, we check the performance of the vertical-mixing scheme by changing the scaling factors for convection and for vertical diffusion both from 1.0 (standard case) to 0.25 (cf. Keeling et al., 1989, Heimann, 1995). The effect on vertical transport can be assessed by comparing seasonal cycles at Mauna Loa (MLO), at 3397 m height, to Cape Kumukahi (KUM), at sea level, both on Hawaii. The observed seasonal amplitude at MLO is about $16 \pm 5\%$ smaller than at KUM. In the standard case we simulate 19% less amplitude at MLO than at KUM, whereas the figure is 33% when the scaling factors are reduced, indicating satisfactory performance of the vertical-mixing scheme in the standard case.

## 5. Discussion

### *5.1. Impact of drought stress*

The conclusion drawn in Subsections 4.1 and 4.2 regarding the impact of drought stress is that although drought stress might reduce NPP significantly, this has only little impact on net $CO_2$ fluxes. This can be seen on Fig. 4 for Formulations I and VII, as for Model 2. The figure suggests that a large part of the reduction in NPP is happening in tropical areas as represented by Graphs a and b. In contrast, III and V, which were both rejected, show a marked seasonality of $CO_2$ exchange in the tropical areas of Graphs a and b. Finally, Model 2 agrees qualitatively with Formulation I in displaying a marked simultaneous reduction in both NPP and SR during the dry season, although this reduction is less severe.

The difference in the seasonal exchange for the various formulations is also documented by the global value of the growing season net flux (GSNF), which is defined as the sum of the monthly net $CO_2$ flux for those months where the net flux is into the biosphere, carried out at each grid point, then integrated over the global land area. GSNF is smallest for Formulation I (10.3 GtC), and largest for III and V (14.5 GtC and 14.2 GtC, respectively), with VII lying inbetween (12.8 GtC). Apparently, with Formulation I tropical seasonality is still substantially more suppressed than with Formulation VII. The value for Model 2 (11.2 GtC) is closer to I than to VII. All values are close to but higher than the figure found by Fung et al. (1987), which is 9.3 GtC for a spatial resolution of 4° by 5°. However, a comparison is difficult because the value of GSNF is resolution dependent.

We will now compare annual NPP from Formulations I and VII with a global NPP map by Fung et al. (1983) on the same 7.83 by 10.00 degree grid of the TM2, based on the global vegetation map by Matthews (1983). The comparison, restricted to grid cells with at least 50% land cover, is displayed in Fig. 5. The Fung et al. data have been generated by assigning a uniform value for annual NPP to each vegetation type of the Matthews vegetation map, so that the values are independent of climate or satellite data. Not surprisingly, the correlation of all displayed data points is considerable (I: $r^2 = 0.770$; VII: $r^2 = 0.734$, $n = 201$). However, for the tropical latitudes (15.65° S to 15.65° N, represented by the larger black dots in Fig. 5), the agreement is clearly better with Formulation I than with Formulation VII (I: $r^2 = 0.738$; VII: $r^2 = 0.495$; $n = 28$). It is likely that Formulation VII overestimates NPP in many tropical regions, as the one

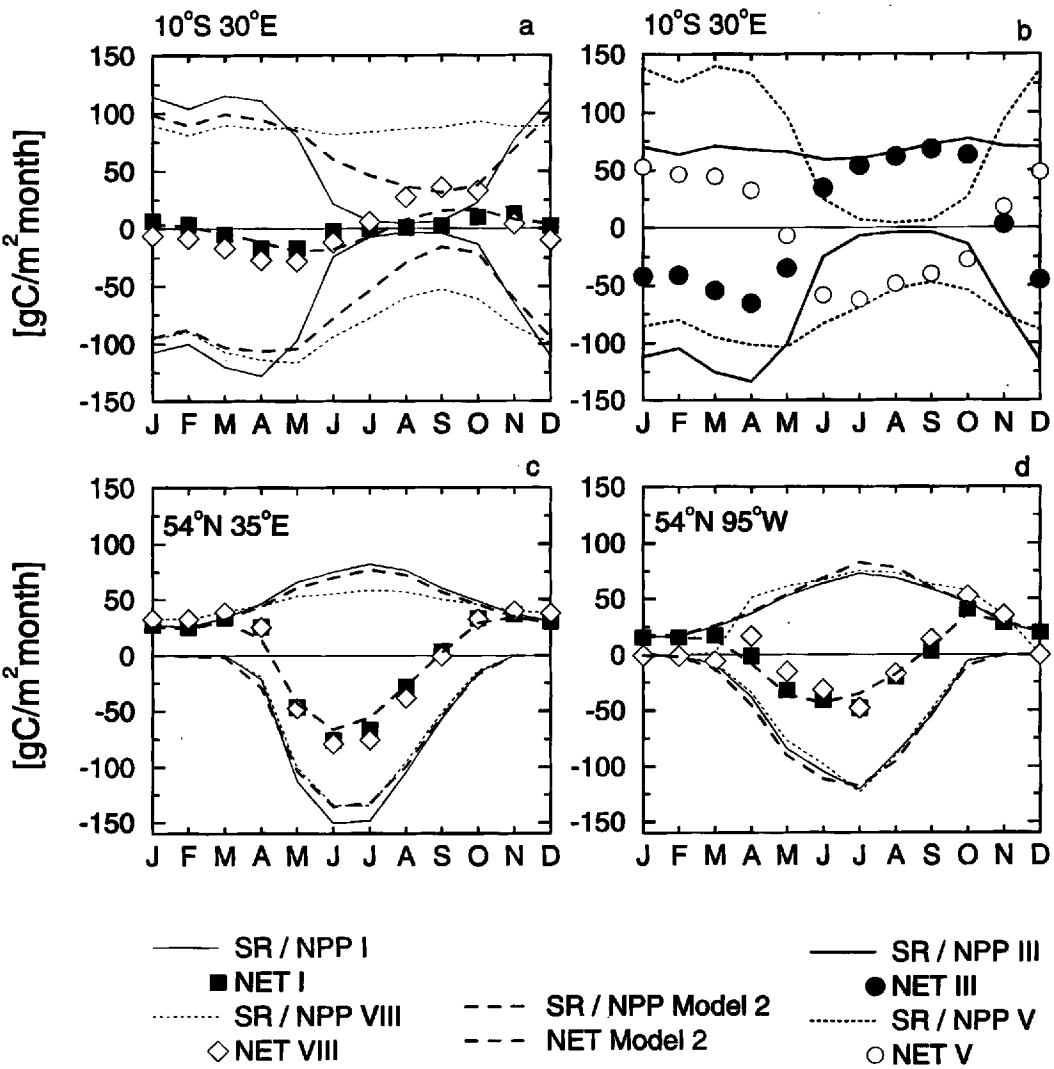


*Fig. 4.* Monthly carbon fluxes, SR ($>0$); NPP ($<0$); net flux (NET), from 3 grid boxes of 4° latitude by 5° longitude. All simulations use a $Q_{10}$ of 1.5, except VIII, where it is 1.2. Coordinates of the grid box centres are indicated in the figure. Graphs a and b show an area with a marked dry season, indicating the different treatment of drought stress in the various formulations of Model 1 and in Model 2. Graphs c and d show fluxes from temperate areas, (d) with a strongly continental climate where the low-temperature cutoff has a marked effect (Formulation VIII). For easy comparison, grid boxes c and d are identical to those used by Fung et al. (1987).

represented by Graphs a and b of Fig. 4, because it does not account for reduced carbon uptake under drought stress that is not severe enough to result in decreased NDVI.

This result, together with the agreement between Formulation I and Model 2 that uses the more physically based Penman-Monteith equation to calculate evapotranspiration, could be considered evidence that Formulation I reproduces atmosphere-biosphere $CO_2$ exchange more realistically than the simple Formulation VII, although drought stress might be overestimated. Evidence from atmospheric $CO_2$ data comes from ASC (Fig. 3), where the September peak in the seasonal cycle

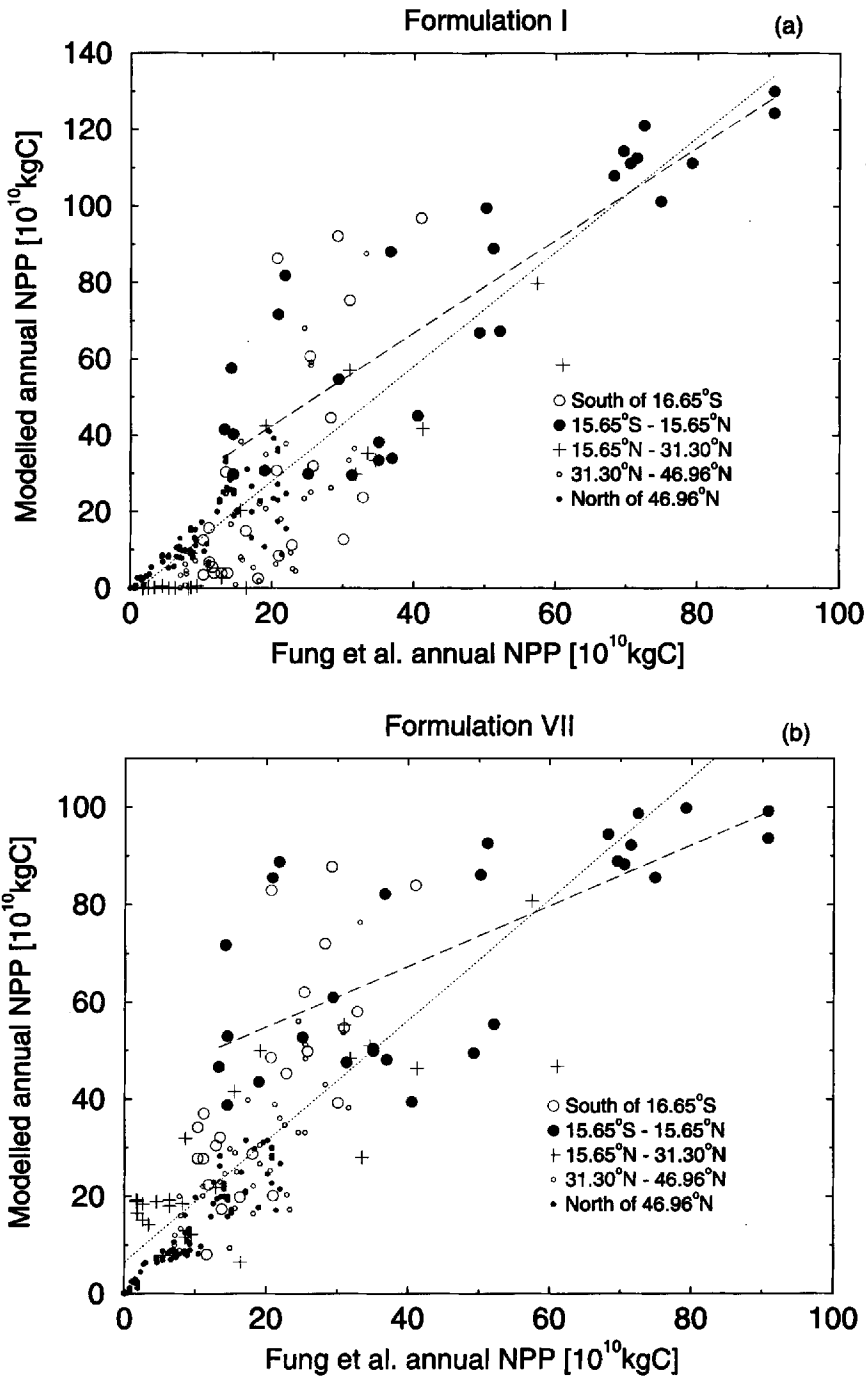


*Fig. 5.* Comparison of the annual NPP at the TM2 resolution from Formulation I (upper graph) and Formulation VII (lower graph) against values by Fung et al. (1983) based on a vegetation map by Matthews (1983). We exclude all grid cells with less than 50% land cover. The straight lines indicate a linear regression of all data points (dotted), or of the points that lie between 15.65° N and 15.65° S (dashed).

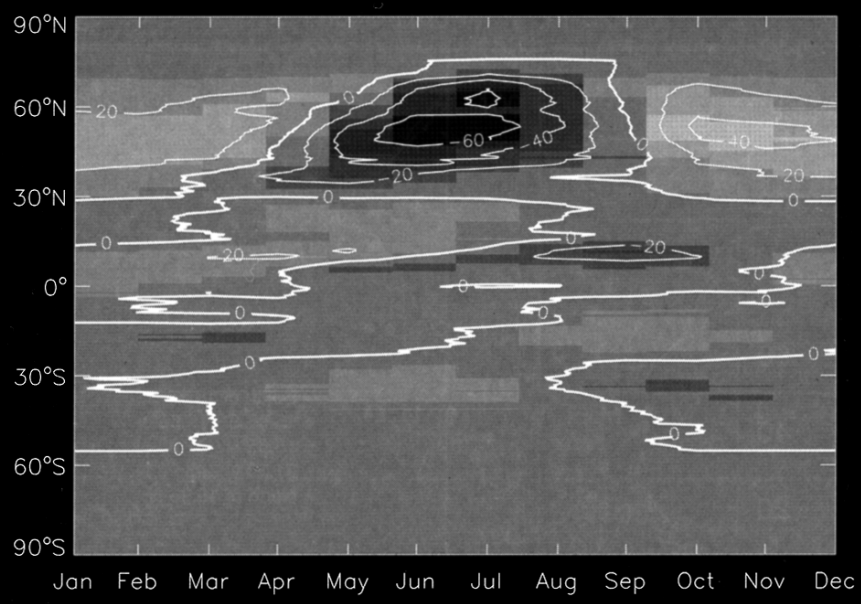


*Fig. 6.* Latitude-time diagram of net biosphere-atmosphere $CO_2$ exchange computed with Model 2. Contour labels are in $10^9$ kgC per month and 1° latitude.

simulated with Formulation VII appears to be too pronounced.

If in fact Formulation I and Model 2 are more realistic, then this implies that the seasonality of tropical $CO_2$ exchange is strongly suppressed because both uptake and release largely happen simultaneously during the wet season. Fig. 6 shows the net $CO_2$ exchange by latitude and month computed with Model 2. Contours indicate the net flux in $10^9$ kg C per month and 1° latitude. Negative values are defined as going into the biosphere and appear dark grey, positive values, appearing light grey, as into the atmosphere. By far the strongest sink region stretches from around 35° N to well into the arctic, and from May to August, starting later at boreal latitudes. The corresponding source from soil respiration is strongest during October and November, after leaf shedding, while temperatures are still relatively high. No net flux of similar size is found in the tropics, although the land area per degree latitude is of similar size as in the temperate and boreal zone. However, a small net sink can be identified that is linked to the wet season. This strong dominance of higher latitudes contrasts with results by Potter et al. (1993) with the CASA model, predicting a net sink of around 20 gC $month^{-1}$ $m^{-2}$ both in summer in northern mid latitudes, and in the wet season in tropical latitudes. A net flux of this size and seasonality in the tropics is predicted by Formulation III, and can be rejected with measurements at ASC, as described in Subsection 4.2. This illustrates how $CO_2$ measurements from tropical stations can be used to test biogeochemical models of the terrestrial biosphere.

A further comment on the suitability of Formulation I and the one-layer bucket model for global vegetation modelling is appropriate. It has been observed that grasslands respond to sinking soil moisture with reduced NDVI (Gao et al., 1992), so that a simple scheme as in eq. (3b) or in Heimann and Keeling (1989), would be appropriate to simulate carbon uptake. This would imply that drought stress is accounted for twice in Formulation I. However, grasses also respond by closing stomata, as apparent from Kim and Verma (1991) and as used in Model 2. For instance, in the study by Kim and Verma, no significant reduction in leaf area index or in the simple-ratio vegetation index (Verma et al., 1993) was observed during a period of drought. In fact, any vegetation shows a double response to drought stress, through stomatal closure and, at varying degrees of stress, through withering. Both effects have been

accounted for in Model 2, by modelling stomatal closure, and through the use of FPAR. Therefore, comparison with Model 2 suggests that qualitatively Formulation I captures the main features of drought-stress impact on NPP, but that this impact is overestimated, partly because vegetation responds less to smaller amounts of soil moisture deficit (as assumed by eqs. (7), cf. Kim and Verma, 1991; Gollan et al., 1985), partly because it does not account for feedbacks between the water and carbon balance.

### 5.2. *Winter-time $CO_2$ release*

In Subsection 4.1, we have concluded that there must be a considerable amount of $CO_2$ released from soils during the winter, from comparing simulations with and without a low-temperature cutoff for $CO_2$ fluxes from soils. The result of such a cutoff can be seen in Fig. 4, Graphs b and d, for temperate vegetation. Note that the value for $Q_{10}$ is only 1.2 for Formulation VIII, but 1.5 for Formulation I. Whereas the cutoff has little impact in regions with a maritime climate (Graph c), the annual course of net $CO_2$ exchange is significantly altered where the climate is strongly continental (Graph d), resulting in a double peak in autumn and spring.

The assumption that there is a significant source of $CO_2$ throughout the whole winter is supported by the results of a number of field studies, where litter decomposition proceeded with no significant slowdown under snow cover (Moore, 1983; Stohlgren, 1988; Taylor and Jones, 1990). The heat insulating property of snow left the soil relatively warm at 0 to $-3$°C compared to air temperatures down to $-35$°C (Moore, 1983). The $CO_2$ produced during litter decay probably escapes fast enough to show up in atmospheric transport as winter-time release. This was found by Solomon and Cerling (1987) who measured $CO_2$ concentrations within soil and snowpack in a montane environment in Utah. However, the field studies mentioned are from sites with a large amount of snowfall compared to the more continental climates of, e.g., the Siberian boreal forest areas. Nonetheless, a smaller amount of snow cover in those latter regions might still be a sufficient insulator to favour bacterial activity in the soil, but be even better at letting $CO_2$ escape to the atmosphere.

## 6. Conclusions and outlook

In this exploration of functional forms of atmosphere-biosphere $CO_2$ exchange, we have found a number of good fits to the observed seasonal cycle of atmospheric $CO_2$. They compare well with those achieved earlier by Heimann et al. (1989) and by Fung et al. (1987). A good fit is achieved by a range of formulations, which illustrates how underdetermined the inversion of atmospheric transport is, even with the highly constrained models used in this study. Limiting factors are fluctuations in the observed seasonal cycle, changes in the wind data, and uncertainties about non-biospheric contributions. We have tried to account for such additional contributions by, e.g., including results from a suitable ocean model (Kurz, 1993). Nonetheless, within those uncertainties, we have shown that measurements of $CO_2$ from suitably located tropical stations can be used as a constraint on modelling the impact of drought stress on biospheric carbon cycling. Remaining difficulties could possibly be overcome by a more accurate resolution of the monsoon circulation, and with the help of accurate data on the ratio of $^{13}CO_2$ to $^{12}CO_2$ that allows us to determine the biospheric contribution to changes in the $CO_2$ concentration (Heimann et al., 1989). Additional measurements of the $O_2/N_2$ ratio in the atmosphere could also be used to verify further the ocean-plankton model of Kurz (1993). Local vegetation effects, that seem to contribute to discrepancies between observations and simulations, might be suppressed by choosing suitably remote measurement locations and by accounting for the selection of certain wind directions from the sea for flask sampling when simulating atmospheric $CO_2$ transport.

Despite these limitations, however, the simple models developed in this study can be tested and parameters can be tuned accurately enough to draw some cautious conclusions about global vegetation activity. Naturally, such a test can be equally applied to more complex, mechanistic terrestrial ecosystem models, so that this study should indicate its scope as well as its limitations. It would be a significant step forward to simulate interannual fluctuations of atmospheric $CO_2$ in the same way as it has been done for the seasonal cycle. Such fluctuations appear to be linked to the El Niño-Southern Oscillation (Keeling et al.,

1989), and possibly to violent volcanic eruptions, such as the recent one of Mount Pinatubo (Sarmiento, 1993). It would require extremely accurate measurements of the carbon isotope ratio of atmospheric $CO_2$ to extract the biospheric contribution to $CO_2$ variations. Such data are not yet available for longer periods. Further, both the vegetation index and the ECMWF weather data used in this study contain inhomogeneities and trends that, because of the delicate balance between carbon uptake and release, dominate interannual carbon flux variations when we run our model interannually. Significant improvements concerning data quality are therefore needed. With such improvements, however, it would be most instructive to compare measured interannual fluctuations in atmospheric $CO_2$ with those derived from a range of model formulations used in this study and those calculated with a number of existing terrestrial-ecosystem models.

## 7. Acknowledgements

The authors wish to thank Jörg Kaduk and Philippe Martin for numerous helpful hints and discussions, and the reviewers for many useful suggestions. In particular, the scheme to computesoil hydraulic properties was obtained from J. Kaduk, and Ph. Martin provided us with a program to simulate the diurnal course of air temperature. Thanks go also to W. Cramer for letting us use his recently improved gridded climatology. The ECMWF data were obtained through Deutscher Wetterdienst, Offenbach, Germany. This work has been funded in part by the European Commission under Contract No. EV5V-CT92-0120.

## 8. Appendix

*The bucket model*

Following is a description of the bucket model used in combination with Model 1. It is a modified version of the one by Prentice et al. (1993), and is based on the theory by Federer (1979), stating that actual evapotranspiration (AET) can be estimated as the lesser of an instantaneous supply and demand function. Demand, equated with potential evapotranspiration (PET), is calculated as the "equilibrium evaporation" rate (McNaughton and Jarvis, 1983) that exists in the limit of a thick boundary layer, where vegetation is aerodynamically decoupled from the atmosphere so that evaporation is driven solely by the amount of available energy:

$$D = \frac{sR}{(s+\gamma)\lambda}. \tag{A1}$$

$D$ is the evaporative demand (kg m$^{-2}$ s$^{-1}$), $R$ the net radiative balance of the canopy (W m$^{-2}$), $s$ the derivative of the saturated vapour pressure with respect to temperature (Pa K$^{-1}$), $\gamma$ the psychrometric constant ($\approx$65 Pa K$^{-1}$), and $\lambda$ the latent heat of vaporization ($\approx 2.5 \times 10^6$ J kg$^{-1}$). $s$, $\lambda$ and $\gamma$ are calculated as in Prentice et al. (1993) from daily mean temperature.

The canopy radiative balance, $R = R_n - G$, is calculated from

$$R_n = 0.85I - 98 \text{ W m}^{-2} \tag{A2}$$

following Stanhill et al. (1972), and

$$G = 0.036R_n, \tag{A3}$$

according to Verma et al. (1986). $R_n$ is the net surface radiation, $I$ incoming solar radiation at the surface, and $G$ the soil flux (W m$^{-2}$). Following Linacre (1968), $I$ is calculated from cloudiness, $n_c$, and top-of-atmosphere solar radiation, $I_{TOA}$:

$$I = (0.75 - 0.5n_c)\, I_{TOA} \tag{A4}$$

$n_c$ is given in fraction of full cloud cover (i.e., $n = 0.3$ means that 30% of the sky is covered by clouds). Computation of $I_{TOA}$ takes account of solar geometry and seasonal variations in sun-earth distance, assuming a solar constant of 1360 W m$^{-2}$. Details can be found again in Prentice et al. (1993). The computed value for $I$ is also used to calculate NPP in Model 1 and $A_u$ in Model 2.

Supply, $S$ (kg m$^{-2}$ s$^{-1}$) is assumed to depend linearly on the amount of extractable soil water:

$$S = C_w w / w_{max}. \tag{A5}$$

$C_w$ is the maximal evapotranspiration rate, $w$ the actual and $w_{max}$ the maximal extractable amount of soil water. $C_w$ is fixed at 1 kg m$^{-2}$ h$^{-1}$ (Federer,

1982). $w_{max}$, the maximum available soil water volume for plant use, is defined as the amount of water that can be extracted from the soil between the field capacity and the wilting point. We assume a matrix potential of 10 kPa and 1500 kPa, respectively. $w_{max}$ is then defined as

$$w_{max} = d(\Theta_f - \Theta_w), \tag{A6}$$

with soil depth, $d$, and volumetric fraction of soil water at field capacity, $\Theta_f$, and at wilting point, $\Theta_w$. The dependence of volumetric soil water fraction, $\Theta$, on matrix potential, $\Psi$, is calculated following Cosby et al. (1984) by the empirical formula

$$\Psi = \Psi_s \left(\frac{\Theta}{\Theta_s}\right)^{-b}, \tag{A7}$$

using $b = 15.7n_{cl} + 3.1$, $\Theta_s = -14.2n_{sa} + 50.5$ and $\log \Psi_s = -0.95n_{sa} + 1.54$. The correlations ($r^2$) found by Cosby et al. are 0.966, 0.771 and 0.809, respectively, using measurements from 11 test sites. $n_{cl}$ and $n_{sa}$ denote fractions of clay and sand in the soil. We use a global data set by Webb et al. (1991) giving such values for various soil horizons. We use horizons of up to one meter depth, assumed as the maximum rooting depth, to sum up the various contributions to $w_{max}$, taking $d$ in eq. (A6) as the depth of each horizon. Additionally, whenever the data by Webb et al. indicate a histosol, that layer is assigned $\Theta_f - \Theta_w = 0.9$.

Monthly input data of temperature, rainfall and cloudiness are interpolated linearly to obtain daily values. The daily course of $I$ is used to integrate AET, i.e., the maximum of $S$ and $D$, analytically over one day. At each daily time step, the difference between rainfall and AET is added to the soil moisture content, $w$. Any amount exceeding $w_{max}$ is lost as runoff. The soil water balance is simulated over several years until a steady state is reached.

## REFERENCES


Arpe, K. 1991. The hydrological cycle in the ECMWF short range forecasts. *Dyn. Atmos. Oceans* **16**, 33–59.

Asrar, G., Myneni, R. B. and Choudhury, B. J. 1992. Spatial heterogeneity in vegetation canopies and remote sensing of absorbed photosynthetically active radiation: a modeling study. *Remote Sens. Environ.* **41**, 85–103.

Bonan, G. B. 1991. Atmosphere-biosphere exchange of carbon dioxide in boreal forests. *J. Geophys. Res.* **96**, 7301–7312.

Brounshtein, A. M., Faber, E. V. and Shashkov, A. A. 1988. *Atmospheric $CO_2$ concentrations derived from flask samples collected at USSR-operated sampling sites.* NDP-033. Oak Ridge/Tennessee: Carbon Dioxide Information Center, Oak Ridge National Laboratory.

CDIAC 1991. *Trends 1991, a compendium of data on global change* (eds. T. A. Boden, R. J. Serpanski and F. W. Stoss). Oak Ridge/Tennessee: ORNL/CDIAC-46, Carbon Dioxide Information Center, Oak Ridge National Laboratory.

Conway, T. J. and Tans, P. 1990. *Atmospheric $CO_2$ concentrations. The NOAA/GMCC flask sampling network.* Oak Ridge/Tennessee: NDP-005/R1, Carbon Dioxide Information Center, Oak Ridge National Laboratory.

Cosby, B. J., Hornberger, G. M., Clapp, R. B. and Ginn, T. R. 1984. A statistical exploration of the relationships of soil moisture characteristics ot the physical properties of soils. *Water Resour. Res.* **6**, 682–690.

Federer, C. A. 1979. A soil-plant-atmosphere model for transpiration and availability of soil water. *Water Resour. Res.* **15**, 555–562.

Federer, C. A. 1982. Transpirational supply and demand: plant, soil, and atmospheric effects evaluated by simulation. *Water Resour. Res.* **18**, 355–362.

Fung, I., Prentice, K., Matthews, E., Lerner, J. and Russel, G. 1983. Three-dimensional tracer model study of atmospheric $CO_2$. Response to seasonal exchanges with the terrestrial biosphere. *J. Geophys. Res.* **88**, 1281–1294.

Fung, I. Y., Tucker, C. J. and Prentice, K. C. 1987. Application of advanced very high resolution radiometer vegetation index to study atmosphere-biosphere exchange of $CO_2$. *J. Geophys. Res.* **92**, 2999–3015.

Gallo, K. P. 1992. *Experimental global vegetation index from AVHRR utilizing pre-launch calibration, cloud and sun-angle screening.* Digital Data. Boulder/Colorado: National Oceanic and Atmospheric Administration, National Geophysical Data Center.

Gao, W., Wesely, M. L., Cook, D. R. and Hart, R. L. 1992. Air-surface exchange of $H_2O$, $CO_2$, and $O_3$ at a tallgrass prairie in relation to remotely sensed vegetation indices. *J. Geophys. Res.* **97**, 18663–18671.

Gollan, T., Turner, N. C. and Schulze, E. D. 1985. The responses of stomata and leaf gas exchange to vapour pressure deficit and soil water content (III). In the sclerophyllous woody species *Nerium oleander. Oecologia* **65**, 356–362.

Heimann, M. 1995. *The global atmospheric tracer model*

*TM2: model description and user Manual.* Hamburg/Germany. Deutsches Klimarechenzentrum (DKRZ), in press.

Heimann, M. and Keeling, C. D. 1989. A three-dimensional model of atmospheric $CO_2$ transport based on observed winds: 2. Model description and simulated tracer experiments. *AGU Monograph* **55**. Washington, American Geophysical Union. 237–275.

Heimann, M., Keeling, C. D. and Tucker, C. J. 1989. A three-dimensional model of atmospheric $CO_2$ transport based on observed winds: 3. Seasonal cycle and synoptic time scale variations. *AGU Monograph* **55**. Washington, American Geophysical Union. 277–303.

Iacobellis, S. F., Frouin, R., Razafimpanilo, H., Somerville, R. C. J. and Piper, S. C. 1994. North African savanna fires and atmospheric carbon dioxide. *J. Geophys. Res.* **99D**, 8321–8334.

Janacek, A., Lüdeke, M. K. B., Kindermann, J., Lang, T. L., Klaudius, A., Otto, R. D., Badeck, F. W. and Kohlmaier, G. H. 1991. A global high resolution mechanistic and prognostic model for the seasonal and long term $CO_2$ exchange between the terrestrial ecosystems and the atmosphere: The Frankfurt Biosphere Model (FBM). Paper presented at the *3rd International Environmental Chemistry Congress* in Salvador-Bahia, Brazil.

Keeling, C. D., Bacastow, R. B., Carter, A. F., Piper, S. C., Whorf, T. P., Heimann, M., Mook, W. G. and Roeloffzen, H. 1989. A three-dimensional model of atmospheric $CO_2$ transport based on observed winds: 1. Analysis of observational data. *AGU Monograph* **55**. Washington, American Geophysical Union. 277–303.

Kim, J. and Verma, S. B. 1991. Modeling canopy stomatal conductance in a temperate grassland ecosystem. *Agric. For. Meteorol.* **55**, 149–166.

Knorr, W., Martin, Ph., Kaduk, J. and Heimann, M. 1995. A coupled carbon and water flux model of terrestrial vegetation: results of a diagnostic modeling study. Hamburg/Germany: *Max-Planck-Institut für Meteorologie Report*, in press.

Kumar, M. and Monteith, J. L. 1981. Remote sensing of crop growth. In: *Plants and the daylight spectrum* (ed. H. Smith). London: Academic Press, 133–144.

Kurz, K. D. 1993. *Zur saisonalen Variation des ozeanischen Kohlendioxidpartialdrucks*. Hamburg/Germany: Max-Planck-Institut für Meteorologie, Examensarbeit Nr. 18.

Leemans, R. and Cramer, W. 1991. *The IIASA climate database for mean monthly values of temperature, precipitation and cloudiness on a terrestrial grid.* RR-91-18. Laxenburg/Austria: Institute of Applied Systems Analysis.

Lieth, H. 1975. Primary production of the major vegetation units of the world. In: *Primary productivity of the biosphere* (eds. H. Lieth and R. H. Whittaker). New York: Springer Verlag.

Linacre, E. T. 1968. Estimating the net-radiation flux. *Agr. Meteorol.* **5**, 49–63.

Los, S. O. 1993. Calibration adjustment of the NOAA AVHRR Normalized Difference Vegetation Index without recourse to component channel 1 and 2 data. *Int. J. Remote Sensing* **14**, 1907–1917.

Matthews, E. 1983. Global vegetation and land use: A new high-resolution data base for climate studies, *J. App. Meteorol.* **22**, 474–487.

McNaughton, K. G. and Jarvis, P. G. 1983. Predicting effects of vegetation changes on transpiration and evaporation. In: *Water Deficit and Plant Growth* (ed. T. T. Kozlowski), pp. 1–47. New York: Academic Press.

Mocrette, J.-J. 1990. Impact of changes to the radiation transfer parameterization plus cloud optical properties in the ECMWF model. *Mon. Wea. Rev.* **118**, 847–873.

Monteith, J. L. 1965. Evaporation and environment. In: *The state and movement of water on living organisms* (ed. C. E. Fogg). Cambridge, UK: Cambridge University Press.

Monteith, J. L. 1977. Climate and the efficiency of crop production in Britain. *Philosophical Transaction of the Royal Society of London* **B281**, 277–294.

Moore, T. R. 1983. Winter-time decomposition in a subarctic woodland. *Arct. Alp. Res.* **15**, 413–418.

Myneni, R. B., Ganapol, B. D. and Asrar, G. 1992. Remote sensing of vegetation canopy photosynthetic and stomatal conductance efficiences. *Remote Sens. Environ.* **42**, 217–238.

Nakazawa, T., Morimoto, S., Aoki, S. and Tanaka, M. 1993. Time and space variations of the carbon isotopic ratio of tropospheric carbon dioxide over Japan. *Tellus* **45B**, 258–274.

Norman, J. M., Garcia, R. and Verma, S. B. 1992. Soil surface $CO_2$ fluxes and the carbon budget of a grassland. *J. Geophys. Res.* **97**, 18845–18853.

Olson, J. S., Watts, J. A. and Allison, L. J. 1983. *Carbon in live vegetation of major world ecosystems.* Oak Ridge/Tennessee: Environmental Sciences Division Publication Number 1997.

Potter, S. C., Randerson, J. T., Field, C. B., Matson, P. A., Vitousek, P. M., Mooney, H. A. and Klooster, S. A. 1993. Terrestrial ecosystem production: a process model based on global satellite and surface data. *Global Biogeochem. Cycles* **7**, 811–841.

Prentice, I. C., Sykes, M. T. and Cramer, W. 1993. A simulation model for the transient effects of climate change on forest landscapes. *Ecol. Modelling* **65**, 51–70.

Prince, S. D. 1991. A model of regional primary productivity for use with coarse resolution satellite data. *Int. J. Remote Sensing* **12**, 1313–1330.

Raich, J. W. and Schlesinger, W. H. 1992. The global carbon dioxide flux in soil respiration and its relationship to vegetation and climate. *Tellus* **44B**, 81–99.

Raich, J. W., Rastetter, E. B., Melillo, J. M., Kicklighter, D. W., Steudler, P. A., Peterson, B. J., Grace, A. L., Moore III, B. and Vörösmarty, C. J. 1991. Potential net primary productivity in South America: application of a global model. *Ecol. Appl.* **1**, 399–429.

Ramonet, M. 1994. *Variabilité du $CO_2$ atmospherique en*

*régions australes: comparaison modèle/mesures.* PhD thesis, University of Paris 7, 295 pp.

Ruimy, A., Saugier, B. and Dedieu, G. 1994. Methodology for the estimation of terrestrial net primary production from remotely sensed data. *J. Geophys. Res.* **99D**, 5263–5283.

Running, S. W. 1984. *Documentation and preliminary validation of H2OTRANS and DAYTRANS, two models for predicting transpiration and water stress in western coniferous forests.* Fort Collins, Colorado: USDA Forest Service Research Paper RM-252.

Running, S. W. and Coughlan, J. C. 1988. A general model of forest ecosystem processes for regional applications. I. Hydrological balance, canopy gas exchange and primary productivity. *Ecol. Modelling* **42**, 125–154.

Running, S. W. and Hunt Jr., E. R. 1993. Generalization of a forest ecosystem model for other biomes, BIOME-BGC, and an application for global-scale model. In: *Scaling processes between leaf and landscape levels* (eds. J. R. Ehlinger and C. Field). New York: Springer Verlag.

Ryan, M. G. 1991. Effects of climate change on plant respiration. *Ecol. Appl.* **1**, 157–167.

Sarmiento, J. L. 1993. Atmospheric $CO_2$ stalled. *Nature* **365**, 697–698.

Sellers, P. J., Berry, J. A., Collatz, G. J., Field, C. B. and Hall, F. G. 1992. Canopy reflectance, photosynthesis, and transpiration (III). A reanalysis using improved leaf models and a new canopy integration scheme. *Remote Sens. Environ.* **42**, 187–216.

Solomon, D. K. and Cerling, T. E. 1987. The annual carbon dioxide cycle in a montane soil: observations, modeling, and implications for weathering. *Water Resour. Res.* **23**, 2257–2265.

Stohlgren, T. J. 1988. Litter dynamics in two Sierran mixed conifer forests. I. Litterfall and decomposition rates. *Can. J. For. Res.* **18**, 1127–1135.

Stanhill, G., Kafkafi, V., Fuchs, M. and Kagan, Y. 1972. The effect of fertilizer application on solar reflectance from a wheat crop. *Israel J. Agric. Res.* **22**, 109–118.

Taylor, B. R. and Jones, H. G. 1990. Litter decomposition under snow cover in a balsam fir forest, *Can. J. Bot.* **68**, 112–120.

Tiedtke, M. 1989. A comprehensive massflux scheme for cumulus parameterization in large-scale models. *Mon. Wea. Rev.* **117**, 1777–1798.

Tucker, C. J. and Sellers, P. J. 1986. Satellite remote sensing of primary production. *Int. J. Remote Sensing* **7**, 1395–1416.

Turner, N. C., Schulze, E.-D. and Gollan, T. 1984. The responses of stomata to vapour pressure deficits and soil water content. I. Species comparison at high soil water contents. *Oecologia* **63**, 338–342.

Verma, S. B., Baldocchi, D. D., Anderson, D. E., Matt, D. R. and Clement, R. J. 1986. Eddy fluxes of $CO_2$, water vapor and sensible heat over a deciduous forest. *Boundary Layer Meteorol.* **36**, 71–91.

Verma, S. B., Sellers, P. J., Walthall, C. L., Hall, F. G., Kim, J. and Goetz, S. J. 1993. Photosynthesis and stomatal conductance related to reflectance on the canopy scale. *Remote Sens. Environ.* **44**, 103–116.

Vogt, K. A., Edmonds, R. L., Antos, G. C. and Vogt, D. J. 1980. Relationships between $CO_2$ evolution, ATP concentrations and decomposition in four forest ecosystems in western Washington. *Oikos* **35**, 72–79.

Webb, R. S., Rosenzweig, C. E. and Levine, E. R. 1991. *A global data set of soil particle size properties.* Digital raster data on 1-degree geographic $180 \times 360$ grid. New York: NASA Goddard Institute of Space Studies.

Wofsy, S. C., Goulden, M. L., Munges, J. W., Fan, S.-M., Bakwin, P. S., Daube, B. C., Bassow, S. L. and Bazzaz, F. A. 1993. Net exchange of $CO_2$ in a mid-latitude forest, *Science* **260**, 1314–1317.